RSC Advances

PAPER

View Article Online
View Journal | View Issue

Cite this: RSC Adv., 2016, 6, 47919

Self-assembled structural transition in L-Arg/H-AOT mixtures driven by double hydrogen bonding†

Xiaoyang Li, Yuanyuan Hu, Wenlong Xu, Guihua Li, Aixin Song* and Jingcheng Hao

Received 21st March 2016
Accepted 7th May 2016

DOI: 10.1039/c6ra07363h

www.rsc.org/advances

The aggregation properties of L-arginine (L-Arg) with the acidic form of sodium bis(2-ethyl-1-hexyl) sulfosuccinate, H-AOT, in water, were investigated in detail. Double hydrogen bonding formed between the guanidyl group on the L-Arg molecule and the $-SO_3H$ group on the H-AOT molecule. The combination of L-Arg and H-AOT through hydrogen bonding and electrostatic interaction led to the self-assembly of the mixtures. The addition of hydrophobic H-AOT to L-Arg solution modulated the hydrophobicity/hydrophilicity of the L-Arg/H-AOT complexes, resulting in an increase of the packing parameter. Accordingly, a transition of the self-assembled structure from micelles to a closed lamellar bilayer structure (vesicles) and then a bicontinuous bilayer structure (sponge phase) occurred. The microstructural transition was reflected by rheological measurements, for which significant changes in both viscosity and elasticity appeared, and this was further confirmed by Cryo-TEM and FF-TEM observations.

1. Introduction

Currently, it is of great interest to study self-assembly systems that may possibly induce the formation of materials with bespoke structures and functions.[1–3] Through modulating the comprehensive weak interactions, including hydrogen bonds,[4–6] π–π stacking,[7,8] electrostatic interactions,[9] hydrophobic interactions[10] and so on, a series of self-assembled structures, such as micelles, vesicles, nanofibers, nanotubes, and liquid crystals,[11–15] can be achieved by varying the concentration and proportion of compounds. With an ever deeper understanding of the self-assembly process and great efforts in the design of the molecules, self-assembly has been proven to be a powerful approach to obtain materials with well-defined structures and controllable functions.[16–18]

Amino acids are a series of essential components for living bodies, having unique advantages in the construction of biocompatible systems.[19] The existence of carboxyl groups and amino groups in their molecules provides great convenience for the synthesis of anionic, cationic, and amphoteric amphiphiles through the introduction of hydrophobic structures, and further to construct different self-assembled structures.[20–23] Among the naturally existing amino acids, L-arginine (abbreviated as L-Arg) is of significant importance because its basic side chain almost always has a $pK_a \geq 12$ and the positively charged planar guanidinium group can work as a hydrogen donor, which provides an avenue to construct the hydrogen bonding driving self-organized structures with anionic amphiphiles.[24] Sodium bis(2-ethyl-1-hexyl)sulfosuccinate (AOT) is a widely used negatively charged amphiphile with double hydrophobic chains and a relatively small hydrophilic group, and can easily form reverse micelles in solvents with weak polarity. Many studies focused on the reverse structures formed by AOT with different metal ions (Na^+, Ag^+, Ca^{2+}, Ni^{2+}, Al^{3+}, In^{3+}, *etc.*) and their use in the synthesis of nanomaterials.[25–30] However, because of the poor solubility, the results of these substances in aqueous solution are relatively less than those in non-aqueous solvents except several reports of AOT and mixtures of AOT with cationic or nonionic additives in aqueous solution.[31–36]

Herein, we prepared the acidic form of AOT, H-AOT, through a simple and fast replacement reaction and extraction process, being different from the usual ion-exchange resin approach, which is generally tedious and fussy for operation. The self-assembly behavior of the mixtures of L-Arg and H-AOT in water was investigated. We focus on this system for three reasons: first, we want to enrich the self-assembled structures formed by AOT-related systems in aqueous solution, for which the acidic form of AOT is fairly rarely used. Second, both L-Arg and AOT are biocompatible components and can be found in some drug carrier and protein delivery systems.[37–39] Third, the acquisition of self-assembled structures by the direct use of amino acids eliminates the need to synthesize the amino acid derived surfactants, being commercially available. In the present system, the self-assembled structural transition from micelles to vesicles, and then to sponge phase were observed with the changing composition. The formation of diverse

Key Laboratory of Colloid and Interface Chemistry & Key Laboratory of Special Aggregated Materials, Shandong University, Ministry of Education, Jinan 250100, China. E-mail: songaixin@sdu.edu.cn; Fax: +86-531-88364750; Tel: +86-531-88363532

† Electronic supplementary information (ESI) available. See DOI: 10.1039/c6ra07363h

aggregates is considered to be driven by the equilibrium of the double hydrogen bonding, electrostatic interaction and the hydrophobicity/hydrophilicity balance, which can be modulated by the proportion of L-Arg to H-AOT.

2. Experimental section

2.1. Materials

Sodium bis(2-ethyl-1-hexyl)sulfosuccinate (AOT) of 98% purity was purchased from Sigma-Aldrich (USA). L-Arginine (L-Arg) was purchased from J&K Chemical Company (China) with the purity of 98%. They were directly used without further purification. Ultrapure water with a resistivity of 18.25 MΩ cm was obtained through a UPH-IV ultrapure water purifier (China).

2.2. Preparation and characterization of H-AOT

H-AOT was prepared through double decomposition reaction. Hydrochloric acid (25 mmol) was added to the diluted aqueous solution of AOT (20 mmol) under stirring at room temperature to confirm the complete transformation of AOT to H-AOT. The slightly turbid solution was obtained containing H-AOT drop with very little size. Then ether was used for the extraction of H-AOT from water because of the insolubility of H-AOT in water. The supernatant ether phase was separated out and was re-extracted by water for several times to eliminate the trace impurities (HCl or NaCl) in ether phase. The target product, H-AOT, was obtained by volatilizing ether. The H-AOT obtained was characterized by ^{1}H NMR (Fig. S1a–c†), EI-MS (Fig. S2†) and FT-IR spectra (Fig. S3†), which demonstrated that H-AOT was prepared successfully.

2.3. Aggregation behavior study

The aggregation behavior was studied by visual inspection with the help of crossed polarizers. Different amounts of H-AOT and L-Arg were mixed in water, then the samples were kept at 25.0 ± 0.1 °C to reach the phase equilibrium.

2.4. Conductivity and pH measurements

The conductivity was measured on a DDSJ-308A (China) conductivity meter with a DJS-1C glass electrode at 25.0 ± 0.1 °C. The pH measurements were performed on a PHS-3C pH meter (China) with an E-201-C glass electrode. The two-phase samples were tested under stirring.

2.5. FF-TEM observations

A small amount of sample solution was mounted onto a specimen holder. Then the specimen holder was plunged into liquid ethane cooled by liquid nitrogen to freeze the sample. Fracturing and replication were performed on a freeze-fracture equipment (EM BAF 060, Leica, Germany) at −170 °C. Pt/C was deposited with an angle of 45° to shadow the replicas, while C was deposited at 90° to consolidate the replica. The replicas were observed in a JEOL JEM-1400 transmission electron microscope operated at 120 kV. The images were recorded on a Gatan multiscan CCD (USA) and processed with a Digital Micrograph.

2.6. Cryo-TEM observation

A controlled environment vitrification system (CEVS) was necessary to prepare Cryo-TEM samples. A micropipette was used to load about 5 μL of solution onto a TEM copper grid coated by carbon-grid support film. The solution was blotted with two pieces of filter paper to form a thin film suspended on the mesh holes. After 5 s, the samples were quickly plunged into liquid ethane (cooled by liquid nitrogen) at −165 °C. Then the vitrified samples were kept in the liquid nitrogen until they were transferred to a cryogenic sample holder (Gatan 626) and examined on JEOL JEM-1400 transmission electron microscope (120 kV) at −174 °C. The images were recorded on a Gatan multiscan CCD (USA) and processed with a Digital Micrograph.

2.7. Rheological measurements

Rheological measurements were carried out on a HAAKE RS6000 rheometer with a coaxial cylinder sensor system (Z41 Ti). In oscillatory measurements, a stress sweep at a fixed frequency of 1 Hz was carried out prior to the following frequency sweep in order that the selected stress was in the linear viscoelastic region.

2.8. FT-IR characterization

The FT-IR measurements were performed on a VERTEX-70/70v FT-IR spectrometer (Bruker Optics, Germany). Taking 64 scans with a final resolution of 4 cm^{-1}, spectra over the range of ν = 4000–400 cm^{-1} was obtained. Spectral manipulation was carried out with the OPUS 6.5 software package (Bruker Optics, Germany). The AOT spectrum was obtained by diluting AOT powder with NaBr powder, while the H-AOT spectrum was obtained by putting H-AOT (liquid) on a NaBr window plate.

3. Results and discussion

3.1. Aggregation behavior

The phase diagram of the L-Arg/H-AOT system was conducted at 25.0 ± 0.1 °C, as shown in Fig. 1. At a fixed L-Arg concentration, one can observe a phase sequence of aqueous solution, L_1 phase, L_1/L_α two-phase, L_α phase, and sol/oil two-phase with the addition of H-AOT. Within the L_α phase region, a gradual transition from $L_{\alpha v}$ phase (vesicle phase) to L_3 phase (sponge phase) occurs with increasing H-AOT concentration at the concentration of L-Arg exceeding 150 mmol L^{-1}, which is further confirmed by Cryo-TEM and FF-TEM measurements.

In order to provide more information on the self-assembly behavior, typical samples were selected for detailed study. Fig. 2 and 3 show the phase transition at $c_{\text{L-Arg}}$ = 300 mmol L^{-1} with the increase in H-AOT concentration. As shown in Fig. 2a, L-Arg solution is transparent with very weak Tyndall effect. We consider that only primary aggregates are formed because the hydrophobic dye, Sudan II, cannot be dissolved in the solution (Fig. S4†), which is similar to the lysine solution.[40,41] When H-AOT is added, L-Arg solution can dissolve H-AOT (below 5 mmol L^{-1})

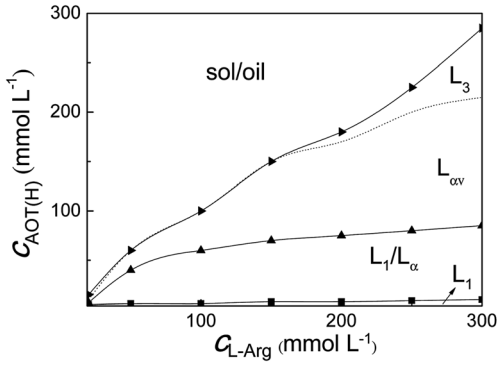

Fig. 1 Phase diagram of L-Arg/H-AOT/H_2O system at 25.0 ± 0.5 °C.

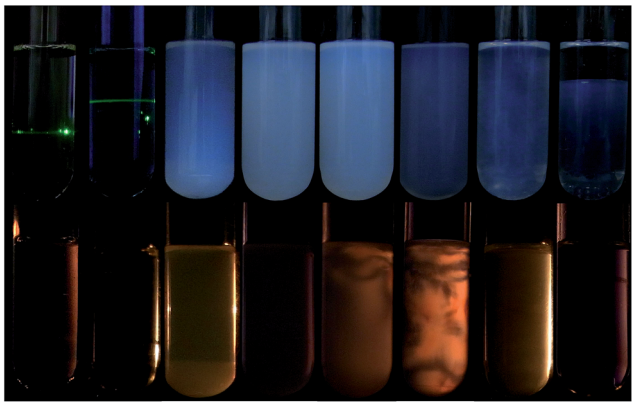

Fig. 2 Photos of typical samples without (up) and with (below) crossed polarizers. The $c_{L\text{-}Arg}$ is 300 mmol L^{-1} and $c_{H\text{-}AOT}$ (from left to right) is: 0, 5, 25, 100, 150, 180, 220, 300 mmol L^{-1}. T = 25.0 ± 0.5 °C.

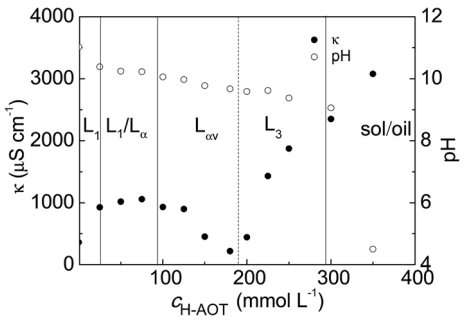

Fig. 3 Phase transition of L-Arg/H-AOT/H_2O system at $c_{L\text{-}Arg}$ = 300 mmol L^{-1} with changing $c_{H\text{-}AOT}$. Conductivity data and pH values are inserted. T = 25.0 ± 0.5 °C.

to form transparent L_1 phase solution, which exhibits Tyndall effect and can solubilize Sudan II in solution (Fig. S4†). After the L_1 phase, a L_1/L_α two-phase region occurs until the concentration of H-AOT reaches about 90 mmol L^{-1}. When H-AOT is in the range of about 90–290 mmol L^{-1}, a slightly turbid L_α phase with birefringence appears. The birefringent texture of L_α phase samples changes with H-AOT concentration, indicating the transition of the microstructures. Within the L_α phase, at first the birefringence becomes stronger with the increasing amount of H-AOT because of the continuous formation of the vesicles, and then becomes very weak. Further study demonstrates that, within the L_α phase region, a gradually transition from vesicles ($L_{\alpha v}$ phase) to sponge structure (L_3 phase) occurs. On further addition of H-AOT, the excess H-AOT dissolves in the hydrophobic region of the bilayers. When H-AOT reaches the saturation of the bilayers, a phase separation occurs and a sol/oil two-phase can be observed.

The conductivity and pH data also reflect the microstructural transition, as shown in Fig. 3. The 300 mmol L^{-1} L-Arg shows a rather high pH of 11.08 due to the basic guanidine and amino groups in L-Arg molecule. With the addition of H-AOT, the pH value decreases gradually because of the acidic –SO_3H group on H-AOT molecule. The conductivity exhibits a complicate case compared with the pH change. The conductivity of L-Arg solution is very low due to the salt-free system and low ionization degree of L-Arg, that is, almost no inorganic ions exist except H^+ and OH^- ions from L-Arg and water. When H-AOT is added, the conductivity starts to increase in aqueous solution and L_1 phase because of the increasing ions concentration induced by the transition of L-Arg from zwitterionic form to cationic form with the addition of H-AOT. It can be observed the conductivity increases with a smaller slope in L_1/L_α two-phase region, which can be considered that the formation of vesicles reduces the trend of conductivity increase because the ions can be trapped in the water layers and cores of vesicles, that weakens the conductive capability. For the same reason, the conductivity decreases sharply in $L_{\alpha v}$ phase and keeps the rather low values. When L_3 phase appears, the conductivity increases due to the formation of bicontinuous structure, in which the ions can move more freely than in vesicles.

The Cryo- and FF-TEM images in Fig. 4 show the detailed microstructural transition of the $L_{\alpha v}$ phase at $c_{L\text{-}Arg}$ = 300 mmol L^{-1} with the variation of H-AOT concentration. When $c_{H\text{-}AOT}$ = 180 mmol L^{-1}, as shown in Fig. 4a, polydisperse vesicles with diameters from about 50 nm to near 300 nm are clearly observed. The solution contains unilamellar and multilamellar vesicles. The vesicles are found to be slightly deformed, indicating the flexibility of the vesicle bilayers, which is often found in hydrocarbon surfactant systems.[42] When H-AOT concentration increases to 220 mmol L^{-1}, three-dimensional network structures of spherical and ellipsoidal objects (Fig. 4b) are formed, which is the characteristic of sponge structure. The

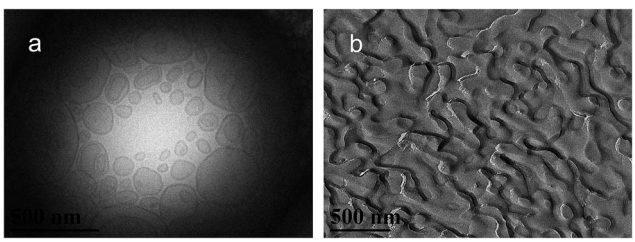

Fig. 4 (a) Cryo-TEM image of sample of 180 mmol L^{-1} H-AOT/300 mmol L^{-1} L-Arg and (b) FF-TEM image of sample of 220 mmol L^{-1} H-AOT/300 mmol L^{-1} L-Arg. T = 25.0 ± 0.5 °C.

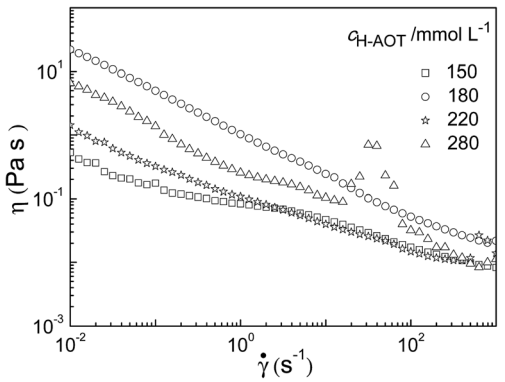

Fig. 5 Viscosity as a function of shear rate of samples at $c_{L\text{-}Arg} = 300$ mmol L^{-1} with different $c_{H\text{-}AOT}$: 150, 180, 220, 280 mmol L^{-1}. $T = 25.0 \pm 0.5$ °C.

sponge structure comprised highly interconnected bicontinuous bilayers and did not show long-range order and birefringence in the static state, which is different from lamellar phase.[14,43]

3.2. Rheological properties

Rheology can provide much detailed information about surfactant self-assembled structures in solution. Fig. 5 shows the steady shear results of L_α phase samples of $c_{L\text{-}Arg} = 300$ mmol L^{-1}. For $L_{\alpha v}$ phase of $c_{H\text{-}AOT}$ from 90 mmol L^{-1} to 190 mmol L^{-1}, the samples exhibit the shear thinning behavior over the studied shear-rate range, which is typical for vesicle phase solution. When $c_{H\text{-}AOT}$ is within the range of 190–290 mmol L^{-1}, L_3 phase samples perform partial shear thickening behavior, which should be attributed to the structural transition from sponge structure to vesicles induced by the input of shear force.[40,44] For further observation, one can find that for sample of $c_{H\text{-}AOT} = 220$ mmol L^{-1}, the shear thickening region appears at a rather high shear rate region, 400–600 s^{-1}, while for sample of $c_{H\text{-}AOT} = 280$ mmol L^{-1}, the shear thickening region shifts to a lower shear rate region, 10–40 s^{-1}, indicating that the more perfect sponge structure formed at 280 mmol L^{-1} than 220 mmol L^{-1}, for which the transition can be achieved at weaker shear force.

The viscoelastic property can be reflected by the dynamic rheological measurements. The oscillatory shear results of the L_α phase is shown in Fig. 6. At $c_{H\text{-}AOT} = 150$ mmol L^{-1}, the viscous modulus G'' exceeds the elastic modulus G' over the studied frequency, indicating a viscous dominant property. When H-AOT concentration reaches 180 mmol L^{-1}, both the G' and G'' increase with the elastic property being dominant. The reason is contributed to the continuous formation of vesicles with the addition of H-AOT, which results in the increase of the density of vesicles and viscoelasticity. With the further addition of H-AOT, the transition from vesicles to sponge structures leads to the rather low viscoelasticity (Fig. 6c and d), which also presents an increasing property with the increase in H-AOT concentration.

3.3. Discussion

Scheme 1 shows the interactions between L-Arg and H-AOT in aqueous solutions. The formation of bilayer structures is driven by the synergistic effect of double hydrogen bonding, electrostatic interaction, and hydrophobic interaction between L-Arg and H-AOT molecules. L-Arg is an alkaline amino acid and exits in its protonated form (Fig. 7a) in aqueous solution, which can easily form double hydrogen bonding with, such as, phosphate, carboxylate, and sulfate, *etc.*[45] When H-AOT is added to L-Arg

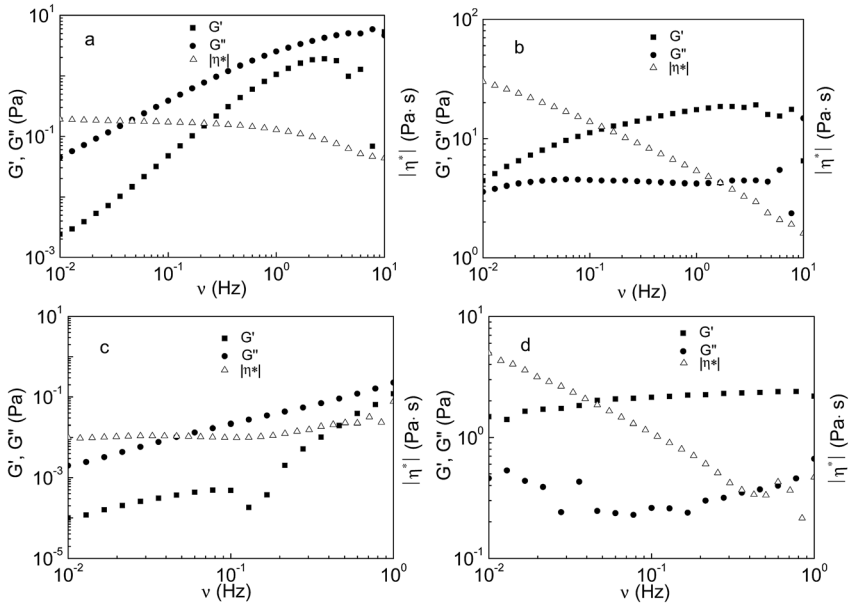

Fig. 6 Dynamically rheological data of four selected samples in L_α phase. $c_{L\text{-}Arg}$ is 300 mmol L^{-1}, and $c_{H\text{-}AOT}$ is (a) 150, (b) 180, (c) 220, and (d) 280 mmol L^{-1}. $T = 25.0 \pm 0.5$ °C.

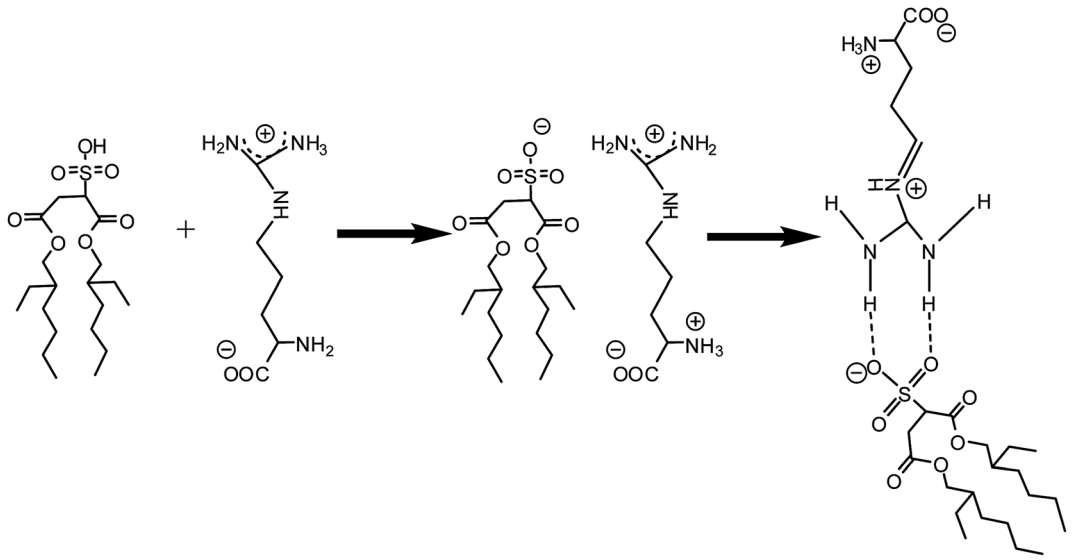

Scheme 1 Schematic representation of the weak interactions between L-Arg and H-AOT molecules.

solution, the $-NH_2$ groups connecting to the –COOH groups on L-Arg molecules are protonated by the H^+ ions dissociated from H-AOT molecules to form $-NH_3^+$ and further form ion pairs with deprotonated H-AOT molecules through the electrostatic interaction. Besides, another type of short-range interaction, the double hydrogen bonding, forms between the H-AOT molecule and the guanidyl group on L-Arg molecule, which can be detected by FT-IR spectroscopy. As shown in Fig. 8, one can only find the COO^- stretching band at 1678 cm^{-1} in L-Arg solution (curve a), no carbonyl stretching band at about 1700 cm^{-1} can be observed because of the dissociation of H^+ from the –COOH group. The guanidyl group (Fig. 7b) on L-Arg molecule is protonated by the dissociated H^+ (Fig. 7c). In the range of 3300–3500 cm^{-1}, there are three peaks which can be ascribed to the stretching mode of the $-NH_2$ group (connecting to the –COOH group) and the –NH– on guanidyl group. With the addition of H-AOT, the $-NH_2$ group was protonated by the H^+ dissociated from H-AOT. This process leads to a FT-IR absorption transition from three peaks to a single peak, which can be ascribed to the stretching mode of the –NH– on guanidyl group. What's more, the bending vibrational mode of the N–H group at 1625 cm^{-1} (line AB) shifts to 1674 cm^{-1} (line CD). This

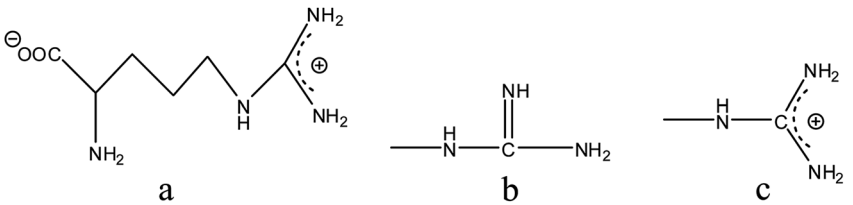

Fig. 7 (a) The protonated form of L-Arg molecule, (b) the guanidyl group on L-Arg molecule and (c) the protonated form of guanidyl group.

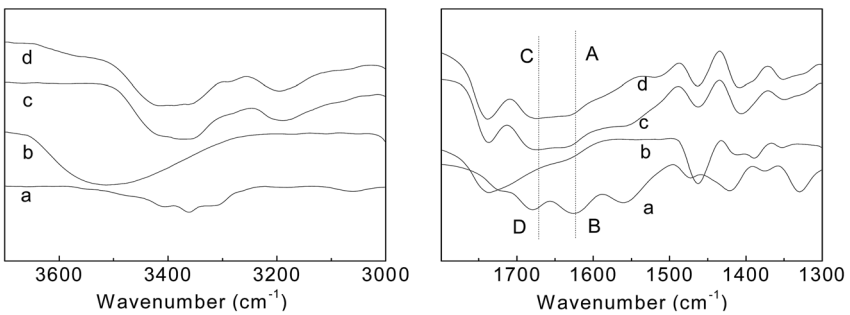

Fig. 8 FT-IR spectra of (a) L-Arg, (b) H-AOT, (c) 180 mmol L^{-1} H-AOT/300 mmol L^{-1} L-Arg, and (d) 280 mmol L^{-1} H-AOT/300 mmol L^{-1} L-Arg. $T = 25.0 \pm 0.5$ °C.

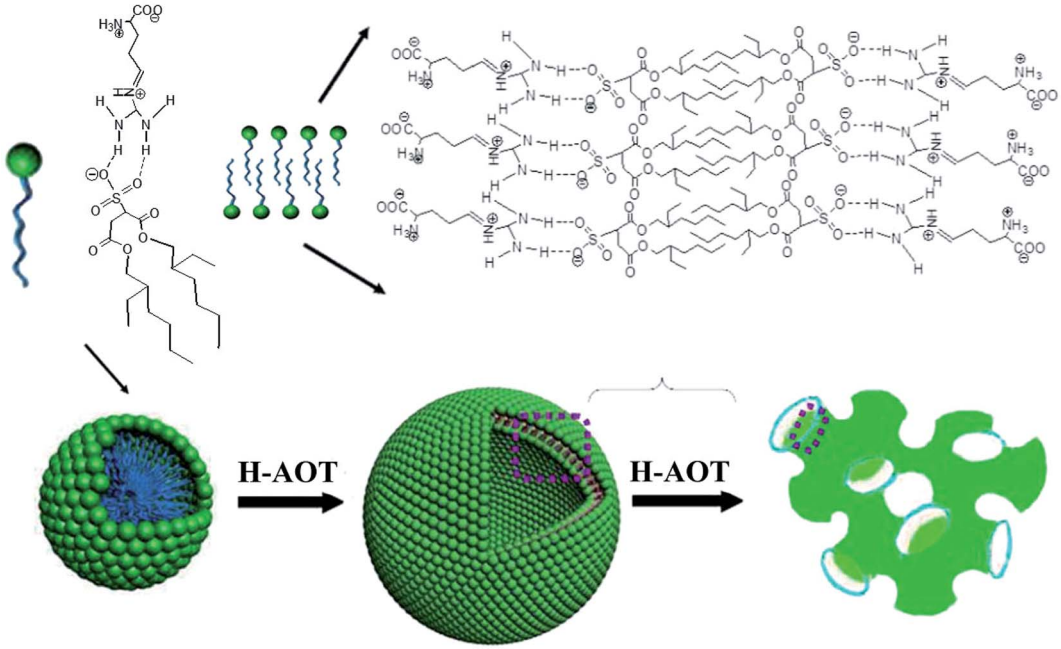

Scheme 2 Schematic representation of micelles, vesicles, and sponge structure in L-Arg/H-AOT.

hypsochromic shift is caused by the formation of double hydrogen bonds between the L-Arg and H-AOT molecules, which prohibits the bending vibrational mode of N–H group. Therefore, we can conclude the main driving force for the formation of the self-assembled structures is double hydrogen bonding.

Thus, the transition of the self-assembled structures with the addition of H-AOT to L-Arg solution is proposed. The L-Arg molecules form primary aggregates in aqueous solution. When hydrophobic H-AOT is added, the ion pairs formed by L-Arg and H-AOT molecules through the double hydrogen bonding and electrostatic interaction reduces the polar area and increases the hydrophobicity of the L-Arg/H-AOT complexes, resulting in the increase of packing parameter, $p = v/(al)$, which is widely applied in the amphiphilic self-assemblies in aqueous solutions. With the further addition of H-AOT, the amounts of the ion pairs increase continuously and modulate the comprehensive effect of electrostatic interaction, hydrogen bonding, and hydrophobicity/hydrophilicity, inducing an increase of p, which leads to the trend of forming larger aggregates with lower curvatures. Thus, the phase transition process, from L_1 phase (micelles) to $L_{\alpha v}$ phase (closed bilayers) and then to L_3 phase (bicontinuous sponge structure), appears, as shown in Scheme 2.

4. Conclusions

In conclusion, a simple and easy extract method to prepare the acidic form of AOT, H-AOT, was reported in this paper, for which the tedious ion-exchange process was avoided. Ascribed to the acidic $-SO_3H$ group and the double hydrophobic chain of H-AOT, rich aggregation behaviors were observed in aqueous solutions of H-AOT mixed with a basic amino acid, L-Arg, at different proportions. The addition of H-AOT to L-Arg solution led to a series of microstructural transitions with a phase sequence of L_1 phase, $L_{\alpha v}$ phase and L_3 phase driven by the synergistic effect of the double hydrogen bonding, electrostatic interaction and hydrophobic effect, which reduces the area of polar groups and changes the packing parameter. Considering the biocompatibility of L-Arg and H-AOT, we hope that our results may contribute to the fundamental understanding of aggregation property induced by H-AOT and be useful for the construction of surfactant complexes in practical applications of biochemical science, extraction technology and other related areas.

Acknowledgements

This work was funded by the NSF for Distinguished Young Scholars of Shandong Province (JQ201303) and National Natural Science Foundation of China (21573134 and 21420102006).

References

1 R. F. Service, *Science*, 2005, **309**, 95.
2 R. Dong, J. Wu, S. Dong, S. Song, F. Tian and J. Hao, *Chem.–Asian J.*, 2013, **8**, 1863–1872.
3 J. Lehn, *Angew. Chem., Int. Ed.*, 2013, **52**, 2–17.
4 J. D. Hartgerink, E. Beniash and S. I. Stupp, *Science*, 2001, **294**, 1684–1688.
5 R. C. Claussen, B. M. Rabatic and S. I. Stupp, *J. Am. Chem. Soc.*, 2003, **125**, 12680–12681.
6 L. Jiang, M. Deng, Y. Wang, D. Liang, Y. Yan and J. Huang, *J. Phys. Chem. B*, 2009, **113**, 7498–7504.

7 D. Ranganathan, V. Haridas, R. Gilardi and I. L. Karle, *J. Am. Chem. Soc.*, 1998, **120**, 10793–10800.
8 J. L. Mynar, T. Yamamoto, A. Kosaka, T. Fukushima, N. Ishii and T. Aida, *J. Am. Chem. Soc.*, 2008, **130**, 1530–1531.
9 I. Willerich and F. Gröhn, *Angew. Chem., Int. Ed.*, 2010, **49**, 8104–8108.
10 J. Israelachvili and R. Pashley, *Nature*, 1982, **300**, 341–342.
11 E. K. Chung, E. Lee, Y. Lim and M. Lee, *Chem.–Eur. J.*, 2010, **16**, 5305–5309.
12 E. T. Pashuck and S. I. Stupp, *J. Am. Chem. Soc.*, 2010, **132**, 8819–8821.
13 J. Douliez, C. Gaillard, L. Navailles and F. Nallet, *Langmuir*, 2006, **22**, 2942–2945.
14 H. Wang, S. Song, J. Hao and A. Song, *Chem.–Eur. J.*, 2015, **21**, 12194–12201.
15 F. Zhang, Z. Xu, S. Dong, L. Feng, A. Song, C. Tung and J. Hao, *Soft Matter*, 2014, **10**, 4855–4862.
16 S. Song, H. Wang, A. Song and J. Hao, *Chem.–Asian J.*, 2014, **9**, 245–252.
17 R. H. Zha, Y. S. Velichko, R. Bitton and S. I. Stupp, *Soft Matter*, 2016, **12**, 1401–1410.
18 D. A. Stone, A. S. Tayi, J. E. Goldberger, L. C. Palmer and S. I. Stupp, *Chem. Commun.*, 2011, **47**, 5702–5704.
19 S. Roy and P. K. Das, *Biotechnol. Bioeng.*, 2008, **100**, 756–764.
20 J. Sen and A. Chaudhuri, *Bioconjugate Chem.*, 2005, **16**, 903–912.
21 R. O. Brito, E. F. Marques, P. Gomes, S. Falcão and O. Söderman, *J. Phys. Chem. B*, 2006, **110**, 18158–18165.
22 L. Sánchez, M. Mitjans, M. R. Infante, M. T. García, M. A. Manresa and M. P. Vinardell, *Amino Acids*, 2007, **32**, 133–136.
23 A. S. Malamas, M. Gujrati, C. M. Kummitha, R. Xu and Z. R. Lu, *J. Controlled Release*, 2013, **171**, 296–307.
24 C. L. Borders, J. A. Broadwater, P. A. Bekeny, J. E. Salmon, A. S. Lee, A. M. Eldridge and V. B. Pett, *Protein Sci.*, 1994, **3**, 541–548.
25 J. Eastoe, T. F. Towey, B. H. Robinson, J. Williams and R. K. Heenan, *J. Phys. Chem.*, 1993, **97**, 1459–1463.
26 E. Caponetti, D. Chillura-Martino, F. Ferrante, L. Pedone, A. Ruggirello and V. T. Liveri, *Langmuir*, 2003, **19**, 4913–4922.
27 D. Fioretto, M. Freda, S. Mannaioli, G. Onori and A. Santucci, *J. Phys. Chem. B*, 1999, **103**, 2631–2635.
28 S. Das and P. V. Kamat, *J. Phys. Chem. B*, 1999, **103**, 209–215.
29 S. Thachepan, M. Li, S. A. Davis and S. Mann, *Chem. Mater.*, 2006, **18**, 3557–3561.
30 J. Lang, A. Jada and A. Malliaris, *J. Phys. Chem.*, 1988, **92**, 1946–1953.
31 A. Song and J. Hao, *J. Colloid Interface Sci.*, 2011, **353**, 231–236.
32 R. Dong, Z. Zhong and J. Hao, *Soft Matter*, 2012, **8**, 7812–7821.
33 Y. Fan, Y. Li, G. Yuan, Y. Wang, J. Wang, C. C. Han, H. Yan, Z. Li and R. K. Thomas, *Langmuir*, 2005, **21**, 3814–3820.
34 I. M. Umlong and K. Ismail, *J. Colloid Interface Sci.*, 2005, **291**, 529–536.
35 B. P. Binks, *Colloids Surf., A*, 1993, **71**, 167–172.
36 S. Nave, J. Eastoe and J. Penfold, *Langmuir*, 2000, **16**, 8733–8740.
37 A. N. Shirazi, N. S. El-Sayed, D. Mandal, R. K. Tiwari, K. Tavakoli, M. Etesham and K. Parang, *Bioorg. Med. Chem. Lett.*, 2016, **26**, 656–661.
38 A. Apicella, P. Heunemann, S. Bolisetty, M. Marascio, A. G. Graf, L. Garamszegi, R. Mezzenga, P. Fischer, C. J. Plummer and J. Månson, *PLoS One*, 2015, **12**, 1–13.
39 A. D. Holmkvist, A. Friberg, U. J. Nilsson and J. Schouenborg, *Int. J. Pharm.*, 2016, **499**, 351–357.
40 G. Li, Y. Liu, W. Xu, A. Song and J. Hao, *J. Phys. Chem. B*, 2014, **118**, 14843–14851.
41 G. Li, L. Feng, P. Zhao, W. Xu, Y. Wang, A. Song and J. Hao, *J. Colloid Interface Sci.*, 2014, **431**, 233–240.
42 S. Song, Q. Zheng, A. Song and J. Hao, *Langmuir*, 2012, **28**, 219–226.
43 A. Zapf, R. Beck, G. Platz and H. Hoffmann, *Adv. Colloid Interface Sci.*, 2003, **100–102**, 349–380.
44 S. Song, H. Wang, A. Song, S. Dong and J. Hao, *Chem.–Eur. J.*, 2014, **20**, 9063–9072.
45 E. Courvoisier, P. A. Williams, G. K. Lim, C. E. Hughes and K. D. M. Harris, *Chem. Commun.*, 2012, **48**, 2761–2763.